Test Results of Two European ITER TF Conductor Samples in SULTAN

P. Bruzzone, M. Bagnasco, M. Calvi, F. Cau, D. Ciazynski, A. della Corte, A. Di Zenobio, L. Muzzi, A. Nijhuis, E. Salpietro, L. Savoldi Richard, S. Turtù, A. Vostner, R. Wesche, and R. Zanino

***Abstract*—Four Nb_3Sn conductor lengths were prepared according to the ITER TF conductor design and assembled into two SULTAN samples. The four lengths are not fully identical, with variations of the strand supplier, void fraction and twist pitch. Lower void fractions improve the strand support and increased twist pitches also lower the strand contact pressure but both tend to increase the AC loss and the lower void fraction also increases the pressure drop so that the mass flow rate in the strand bundle area of the cable is reduced.**

The assembly procedure of the two samples is described including the destructive investigation on a short conductor section to assess a possible perturbation of the cable-to-jacket slippage during the termination preparation.

Based on the DC performance and AC loss results from the test in SULTAN, the impact of the void fraction and twist pitch variations is discussed in view of freezing the ITER conductor design and large series manufacture. A comparison with the former generation of conductors, using similar strands but based on the ITER Model Coil layout, is also carried out.

The ITER specifications, in terms of current sharing temperature, are fulfilled by both samples, with outstanding results for the conductor with longer twist pitches.

***Index Terms*—Cable-in-conduit conductor, ITER, Nb_3Sn strand.**

I. Introduction

AFTER the poor results of the Toroidal Field Advanced Strand (TFAS) samples tested in early 2006 [1], a new generation of samples according to the nominal ITER Toroidal Field (TF) conductor specifications have been designed and tested in SULTAN at PSI Villigen (CH) in 2007 [2].

The European short conductor samples assembled at CRPP and identified as TFPRO1 and TFPRO2 are the first Nb_3Sn cable-in-conduit conductors that have been qualified for the coils of the ITER TF magnet system.

The ITER requirements are fulfilled when the current sharing temperature (T_{cs}) is higher than 5.70 K at the nominal operating conditions. For the TF coils, this corresponds to a current of 68 kA and an effective magnetic field of 11.3 T, (which scales to a 10.78 T background field in SULTAN) [3].

TABLE I
Sample Characteristics

	TFPRO1		TFPRO2	
	EAS1	EAS2	OST1	OST2
Strand diameter [mm]	0.81			
Cu: non- Cu in strand	0.91		1	
Manufacturing technology	Bronze route		Internal Sn	
Diffusion barrier	Ta			
Non-Cu hyst. loss ±3 T [kJ/m^3]	140		900	600
Jc @4.2 K,12 T [A/mm^2] *	710		1150	1070
Strand n-index, @4.2 K, 12 T *	41		29-31	
Cabling layout	((2 s/c + 1 Cu) × 3 × 5 × 5 + core) × 6			
Core	3 × 4			
Cu strand diameter in triplet	0.82		0.81	0.82
Cu strand diameter in core	0.81			
Final outer diameter [mm]	43.45	42.05	42.05	41.45
Void fraction [%] *	33.8	29.3	29.1	27.7
Twist pitch sequence	45/87.5/126.5/245/460			116/182/245/415/440
# of sc strands	900			
# of copper wires	522			
Heat treatment schedule [°C/h]	210/50+340/25+430/25+575/100+655/100			

*: measured at CRPP

II. Strand, Conductor and Samples Layout

The strand characteristics of the four European CICC short conductor samples are listed in Table I. They are identified with the short name of the supplier: EAS for European Advanced Superconductors and OST for Oxford Superconducting Technology.

The TFPRO1 conductors are made of bronze route EAS Nb_3Sn strands and are characterized by different void fraction; the TFPRO2 "legs" are made of internal Sn OST strands with a similar void fraction but different twist pitches. The choice for longer twist pitches is based on the optimization described in [4]. The principal features of the conductors are also gathered in Table I. Cabling and jacketing was carried out at Luvata Italy [5].

III. Sample Preparation

A. Preliminary Operations

The original conductor lengths are first cut to 3425 mm and the terminations are swaged to a lower void fraction before heat

Manuscript received August 9, 2007. This work, supported by the European Communities under the contract of Association between EURATOM/Swiss, was carried out within the framework of the European Fusion Development Agreement.

P. Bruzzone, M. Bagnasco, M. Calvi, F. Cau, and R. Wesche are with EPFL-CRPP Fusion Technology, Villigen PSI, Switzerland (e-mail: pierluigi.bruzzone@psi.ch; maurizio.bagnasco@psi.ch; marco.calvi@psi.ch; francesca.cau@psi.ch; rainer.wesche@psi.ch).

D. Ciazynski is with CEA Cadarache, Lez Durance, France (e-mail: daniel.ciazynski@cea.fr).

A. della Corte, A. Di Zenobio, L. Muzzi, and S. Turtù are with ENEA, Frascati Italy (e-mail: dellacorte@frascati.enea.it).

A. Nijhuis is with University of Twente, The Netherlands (e-mail: A.Nijhuis@tnw.utwente.nl).

E. Salpietro and A. Vostner are with EFDA, München, Germany (e-mail: ettore.salpietro@tech.efda.org; alexander.vostner@tech.efda.org).

L. Savoldi Richard and R. Zanino are with Politecnico, Torino, Italy (e-mail: laura.savoldi@polito.it; roberto.zanino@polito.it).

Digital Object Identifier 10.1109/TASC.2008.922268

treatment without dismantling the jacket to simplify the preparation of the samples. For EAS1, both ends have been compacted to a 42.7 mm diameter over a length of 450 mm. For the other conductors, whose outer diameter is already smaller than 42.7 mm, no further compaction has been applied.

To prevent any slippage between jacket and cable, two crimping rings are placed at the beginning of the compacted section. The rings are first slid and then compacted to reach locally a void fraction of ∼20%. A 1.5 m long steel rod, with an outer diameter of 6.4 mm, is inserted into the central spiral, with nominal inner diameter of 7 mm, in order to prevent collapsing of the spiral. These reinforcing pipes stay in place during the heat treatment and are welded shut during the termination assembly to force the helium to flow in the strand bundle.

B. Heat Treatment

The heat treatment of the four conductor sections has been carried out at CRPP in a vacuum furnace, with purging Ar gas inside the conductors. The schedule for this treatment is a compromise between the optimum heat treatment for the EAS bronze strands and the OST internal tin strands see Table I.

C. Joint/Termination Assembly

After the heat treatment, strain gauges are applied on the jacket 970 mm from the lower end of the conductor; a first measurement is done and retained as a reference. Afterwards, the jacket is removed from the termination region by a milling machine and then the strain gauges measurement is repeated, in order to verify the residual stress state of the jacket. For both samples, the change of strain at room temperature is zero within the accuracy of the measurements.

The cable wrap is removed whereas the sub-cable wraps are cut only on the outer surface. To remove the Cr strand coating, the conductor ends are lowered in a 16–18% HCl solution in an ultrasonic bath. From the other end of the conductor, N gas is blown to avoid corrosive vapors inside the CICC. When the surface appears free of Cr, the conductor is lifted and washed in a water ultrasonic bath. Both conductor ends are then heated to 240°C and tinned with CASTOTIN 1.

To assemble the upper termination, the conductor is placed in a pre-fabricated (and pre-tinned) open Cu-SS box, where the Cu plate is machined in order to match the cable outer diameter. Sn_5Ag foils are interleaved between cable and Cu plate see Fig. 1. The box is then heated to 280°C under 10 kN load and the lid is welded shut.

For the lower joint the two cable ends are first aligned by means of a vacuum-tight eye-glass piece welded to the jacket and then soldered inside a stainless steel box to segmented Cu elements which cover >90% of the cable perimeter see Fig. 1. Two rows of each 14 Cu saddle-shaped elements interleaved by Teflon spacers build a joint active length of ∼420 mm. After soldering, the lid is welded and the steel box itself is welded to the eye-glass piece.

The electrical insulation is granted by glass-epoxy half shells with access to the instrumentation. To withstand the repulsive force during the test, a SS clamp is bolted with only a slightly pre-load (5 Nm) to prevent deformation of the round conductor.

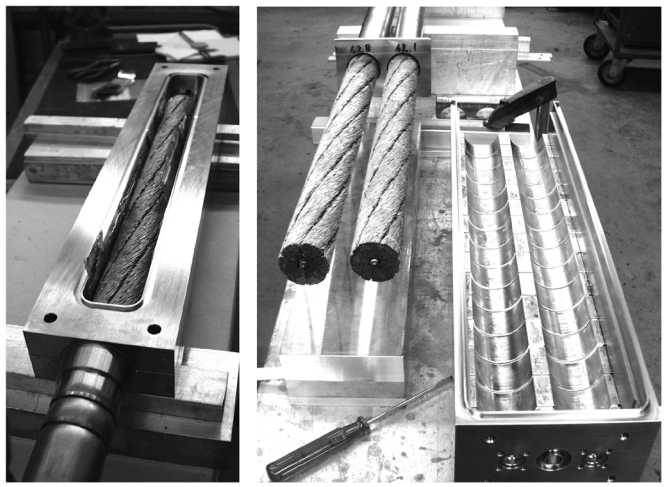

Fig. 1. TFPRO1: upper termination with Sn_5Ag foils before the soldering (left) and pre-tinned conductors with the eye-glass piece and joint box (right) with the lower row of Cu saddle pieces before the soldering.

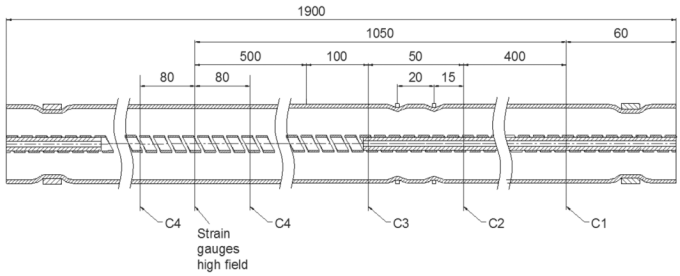

Fig. 2. Strain gauge and cut position along the sample.

D. Cable/Jacket Slippage Measurement

In order to assess the cable/jacket slippage in the SULTAN samples, an additional length (1.9 m) of EAS2 conductor has been used for destructive tests. The short section has been prepared at one end as a regular SULTAN sample termination; at both ends, two 10 mm wide and 3 mm thick steel clamps have been applied to block cable and jacket. The cable is fully compacted, so that the void fraction in the bundle region underneath these clamps is 0%. At about 550 mm from one end, the two standard crimping rings are applied. After the heat treatment, four strain gauges are applied at the location corresponding to the central SULTAN field in a real sample, i.e. about 650 mm away from the crimping rings. The sample is then chopped four times. The location of the cuts C1–C4 is shown in Fig. 2. C1 simply removes the strong clamp at the end, C2 represents the dismantling of the jacket during the joint/termination assembling in a real sample, C3 eliminates the constraint of the crimping rings, C4 (two cuts) further reduces the cable/jacket contact length. The strain gauges are read before the first cut and after each cut. The results are shown in Fig. 3. The small positive strain after the first three cuts is only apparent, because it falls within the error bar; on the contrary, after C4, a relaxation equal to −803 ppm is observed in the steel jacket, in good agreement with the data of JAEA (−630 ppm to −820 ppm) for a full relaxation experiment [6]. Moreover, even after cutting the crimping rings, no change of strain is observed, therefore, the cable/jacket friction over about 600 mm is sufficient to preserve the strain in EAS2.

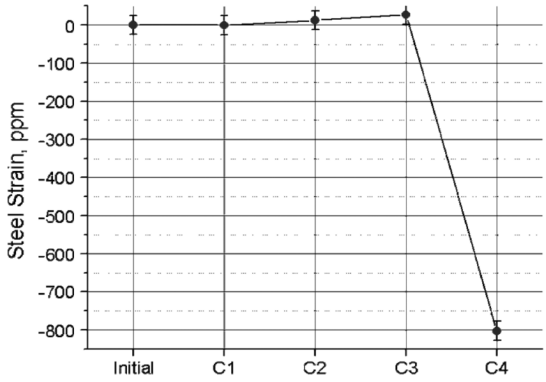

Fig. 3. Evolution of the steel strain, measured by the strain gauges at room temperature.

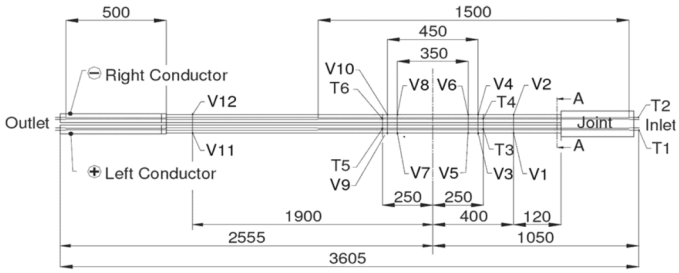

Fig. 4. Sketch of sample instrumentation.

TABLE II
TWENTE STRAND SCALING PARAMETERS

	TFPRO1 EAS	TFPRO2 OST2		TFPRO1 EAS	TFPRO2 OST2
C_1 [AT]	12039	17390	C_{a1}	71.39	81.69
B^*_{c2m} [T]	35.75	34.02	C_{a2}	28.28	35.25
T^*_{cm} [K]	16.52	16.21	$\varepsilon_{0,a}$ [%]	0.25	0.15
			ε_m [%]	–0.12	–0.06

The crimping rings were however applied to all the samples to assure no slippage in case of lower engagement.

E. Instrumentation

The conductor lengths are cooled in parallel by two circuits with independent regulation of mass flow. The flow is upwards from bottom to top. Typically, a mass flow rate of 4 g/s has been used in the DC tests. Fig. 4 shows a sketch of the instrumentation of the TFPRO SULTAN samples indicating the positions of the various voltage taps and temperature sensors.

For the determination of the current sharing temperature, the sensors T5 and T6 immediately after the high field region have been retained. The reference voltage taps (10 $\mu\mathrm{V/m}$ criterion) are the pairs V3–V9 (left leg) and V4–V10 (right leg). At low electric fields, the readings of the temperature sensors before and after the high field region (T3, T5 left leg, T4, T6 right leg) coincide within 0.01 K.

IV. SUMMARY OF TEST RESULTS

A. Strand Scaling

The EAS and OST2 strand critical current are described by the deviatoric strain model developed at Twente University [7], [8] with the scaling parameters listed in Table II.

TABLE III
DURHAM STRAND SCALING PARAMETERS

	TFPRO2 OST1		TFPRO2 OST1
$A(0)$ [$\mathrm{Am^{-2}T^{-3}n^*K^{-2}}$]	4.291×10^7	p	0.9631
B^*_{c2} [T]	29.72	q	2.229
T^*_c [K]	16.71	n^*	2.532
ε_m [%]	0.1371	ν	1.518
c_2	-0.7816	w	2.423
c_3	-0.6318	u	0.1155
c_4	-0.1732		

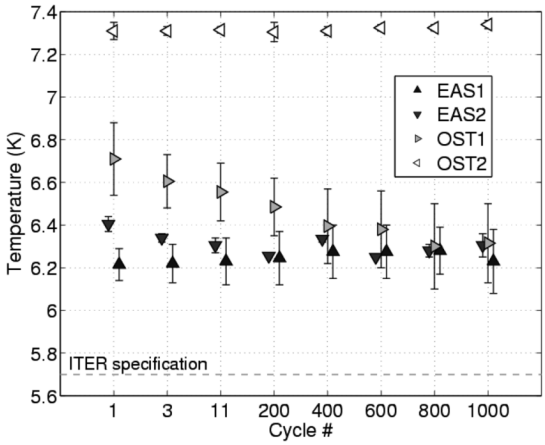

Fig. 5. T_{cs} results as a function of the cyclic load at $\mathrm{I} = 68$ kA and $\mathrm{B} = 10.78$ T. The ITER specification (5.7 K) is also shown.

The OST1 strand was characterized at Durham University with the scaling relations proposed by D. Hampshire in [9]. The derived scaling parameters are reported in Table III.

B. DC Test Results

The main DC tests are performed with a background field of 10.78 T and $I = 68$ kA. In order to assess the performance of the conductors after repeated loads, 1000 EM load cycles are carried out ramping the current from 0 to 68 kA and back in a constant background field of 10.78 T. The T_{cs} was measured in virgin state, at the 3rd, 10th and then after every 200th cycle.

The samples have been further tested after a warm-up/cool-down cycle with the aim of evaluating the impact of a thermal cycle on the conductor performance. In order to clarify the consequences of an overloading, an overload cycle (11 T, 80 kA) was also performed at the end of the DC tests.

Several I_c measurements have been performed at the beginning of the measurement campaign, after 1000 cycling loads, after the warm-up/cool-down cycle and after the overloading to estimate the n-value of the conductors.

The T_{cs} evolution during 1000 cycles is shown in Fig. 5. The error bars come from different voltage post-processing methods (according to [1] or to [2]). Only OST1 presents a rather high early voltage development and the post-processed T_{cs} value is significantly higher than in the raw data. No relevant performance degradation is observed with cyclic load in all the conductors; only for OST1 a reduction of $\sim$0.4 K is observed but the final value is still 0.4 K above the ITER specification. The T_{cs} results have been also benchmarked with calorimetry as described in [2].

TABLE IV
ANALYSIS OF DATA AFTER CYCLING LOAD

		TFPRO1		TFPRO2	
		EAS1	EAS2	OST1	OST2
I (ε)	ε (%)	–0.62	–0.60	–0.57	–0.46
	γ (%/kA T)	0	0.48×10^{-4}	2.14×10^{-4}	0
	n	9	9	6.5	22
	σ (K)	0.04	0.07	0.02	0.07
II (A_r)	ε (%)	–0.62	–0.63	–0.49	–0.46
	A_r	1*	1*	0.535	1*
	n	9	9	6.5	22
	σ (K)	0.04	0.08	0.01	0.07
Mixed	ε (%)	–0.62	–0.59	–0.51	–0.46
	A_r	1	0.908	0.615	1
	γ (%/kA T)	0	0	0.6×10^{-4}	0
	n	9	9	6.5	22
	σ (K)	0.04	0.06	0.001	0.07

*: $A_r = 1$ fixed value.

C. Analysis of DC Results

The comparison between the conductor performances (computed as in [2]) and the strand one has been carried out with the same procedure explained in [1]. A_r here is the ratio between the effective superconductor area and the total ideal superconductor area. The results are gathered in Table IV for the T_{cs} after 1000 cycles. The three approaches give the same results for EAS1 and OST2 with very low sensitivity to the transverse BI load ($|\gamma| < 0.1 \times 10^{-4}\%/\mathrm{kAT}$). In particular, the exceptionally good result of OST2 suggests that the actual longitudinal compressive strain after the cool-down may be lower than the initially assumed value of -0.6%. The reduced void fraction in EAS2 produces limited effect on the conductor performance. The comparison between the OST samples suggests that the improved support given by the longer pitches helps in preventing strand damage ($A_r = 0.6$ vs. 1 in the mixed approach), which assures a much higher n-value, too.

D. AC Test Before and After Cyclic Load

AC loss tests (± 3 T transverse field with frequencies from 0.2 to 2 Hz) are performed in a background field of 2 T before and after the cyclic load. The loss is measured by gas flow calorimetry using the sensors T5 and T6 for the two legs, respectively. As expected, the loss is strongly reduced after the cyclic load see Fig. 6 as a consequence of the adjustment of the strand contacts inside the cable. In EAS2 the lower void fraction is responsible for the 50% higher cable time constant $(n\tau)$ after the cyclic load In OST2, the longer twist pitches and the low void fraction limit the re-adjustment so that the AC loss reduction after cyclic load is less pronounced.

E. Comparison With the TFAS Sample

The EAS1 and OST2 conductors have been compared with the EAS and OST legs of the TFAS1 sample, described in [1], where the only difference is given by the cable layout. In both cases, the current samples show a significant performance improvement quantified in an increase of 1.1 K and 1.5 K in the T_{cs} for the EAS and OST conductors, respectively.

V. CONCLUSION

Two European ITER TF prototype samples were fabricated, assembled and tested in SULTAN. Independent from the exact procedure of the data reduction all four EU conductors not only fulfill the ITER specification but assure an additional temperature margin for normal operation conditions. The reduction of the void fraction from 33% to 29% has limited impact on the DC performance of CICC made of bronze strands, whereas the increased twist pitches allowed exceptional DC results at the cost of significantly higher AC loss in OST2.

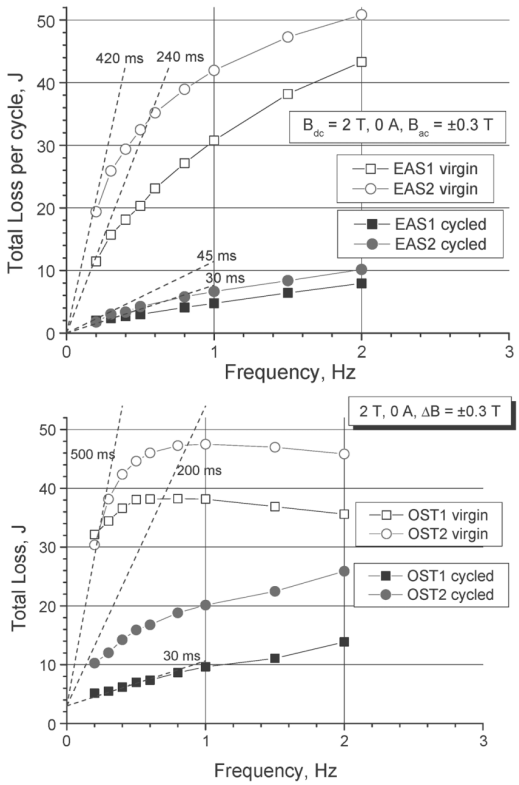

Fig. 6. Evolution of the AC loss (referred to the total strand volume) as a function of the frequency before and after cycling for the TFPRO1 (top) and TFPRO2 (bottom) sample. The $n\tau$ lines are only a guide to the eye.

ACKNOWLEDGMENT

The views and opinions expressed herein do not necessarily reflect those of the European Commission. The technical support of PSI (Paul Scherrer Institute) is greatly acknowledged.

REFERENCES

[1] P. Bruzzone *et al.*, "Test results of two ITER TF conductor short samples using high current density Nb3Sn strands," *IEEE Appl. Supercond.*, vol. 17, no. 2, pp. 1353–1356, 2007.
[2] P. Bruzzone *et al.*, "Results of a new generation of ITER TF conductor samples in SULTAN," presented at the MT-20 Conf., paper 2D01.
[3] D. Bessette and N. Mitchell, "Review of the results of the ITER toroidal field conductor R&D and qualification," presented at the MT-20 Conf., paper 4I11.
[4] A. Nijhuis *et al.*, "Transverse load optimisation in Nb3Sn CICC design; Influence of cabling, void fraction and strand stiffness," *Supercond. Sci. Technol.*, vol. 19, pp. 945–962, 2006.
[5] U. Besi Vetrella *et al.*, "Manufacturing of the ITER TF full size prototype conductor," presented at the MT-20 Conf., paper 4I10.
[6] Y. Nunoya, *JAEA,* . Aug. 2006, private communication.
[7] A. Godeke, "Performance Boundaries in Nb_3Sn Superconductors," PhD Thesis, University of Twente, , 2005, 90-365-2224-2.
[8] A. Godeke *et al.*, "A general scaling relation for the critical current density in Nb_3Sn," *Supercond. Sci. Technol.*, vol. 19, pp. R100–R116, 2006.
[9] D. M. Taylor and D. P. Hampshire, "The scaling law for the strain dependence of the critical current density in Nb_3Sn superconducting wires," *Supercond. Sci. Technol.*, vol. 18, p. 241, 2005.